Technical Report

Microcrack Parameters Characterization in Hard-Coatings Using Moments for Image Processing

A. Femat-Diaz[1,*], *I. Terol-Villalobos*[2], *J. Torres-Gonzalez*[2], *F. Manríquez-Guerrero*[2], *and*
D. Vargas-Vazquez[1]

[1] Universidad Autónoma de Querétaro, Facultad de Ingeniería, División de Estudios de Posgrado.
Cerro de las Campanas s/n, Querétaro, Querétaro 76010, México.
[2] Centro de Investigación y Desarrollo Tecnológico en Electroquímica S.C., Pedro Escobedo,
Querétaro 76700, México.
[*]E-mail: afemat@uaq.mx

The purpose of this paper is to present an automatic, reliable technique to characterize length and orientation of microcracks in hard-coatings that is easy to implement. Consequently subjectivity due to human perception for measuring these characteristics of cracks can be eliminated. This study was done using optical microscope images of hard chromium coatings. For the measurements with image processing, geometric moments, which is a known technique, is useful. However, the segmentation of microcracks plays an important role in making these measurements. In this paper, four samples have been considered, and manual and automated measurements have been performed in order to note the similarities. The results of the automatic method are contrasted with the manual measurements for one image per sample. These results show there was not significant differences between methods. Next, the automatic measurements for groups of seventeen images per sample are compared to analyze differences between samples where there was evidence that a difference between samples existed. Confidence intervals for medians were calculated at 95% confidence. Significance for the differences in samples medians for cracks' length and angle were found to be *p-value <0.001*. Therefore, it was proven that the proposed technique is a very useful tool to characterize length and orientation in microcracks.

1. INTRODUCTION

Surface coatings are used to improve materials' properties such as appearance, physical or mechanical. Chromium coatings are widely used in industry due to its hardness, wear, and corrosion

properties. After fabrication, certain parts may contain surface defects such as scales, pits, mold marks, grinding lines, tool marks, or scratches.

Cracks in coating layers are caused by its re-crystallization process, that changes the structure from hexagonal face centered (hcp) to body centered cubic (bcc). It is known that bright electrodeposits are usually internally stressed, which is noticed in a high hardness. A tensile state of stress in the coating may cause the formation of cracks; chromium coatings have high tensile stress.

Residual stresses are inherent characteristics of electrolytic deposits; they depend on substrate metal, temperature, current density, and chemical concentrations of the electrolyte. Residual stresses can also be produced by plastic deformation heterogeneity during the process of electroplating [1]. They are classified as intrinsic or extrinsic [2]. The intrinsic stresses are developed in the deposit; while extrinsic ones are the result of the interaction of deposit and substrate [3].

It has been found that bright chromium coatings frequently begin to crack when the thickness is between 1 and 3 μm [4-6]. When a crack starts the local current density increases at its edges. Chromium is deposited faster at these edges which closes the crack. This phenomenon repeats in cycles as the deposit grows and closed cracks do not open again [4].

The prediction of structure problems allows the control of their degradation. Consequently, the detection and characterization of cracks on hard coatings is an important step in the fabrication of materials. The development of automated crack detection techniques and accurate methods for crack characterization are important for manufacturing applications.

In hard coatings the most important characteristics for micro-cracks are the length and their perpendicularity to the substrate. Some commercial packages have certain measurements that can be implemented in a semi-automatic or partially automatic way. However, the development of fully automated methods for the measurement of these characteristics is still under investigation.

Only one case where is used a technique to measure crack parameters with image processing was found. In 2005, Grande [7] reported a work where a Y projection to X projection ratio is used to measure vertical crack orientation, provided by Clemex Inc.Vision image analysis software. Also, it is well known in this field that determination of the degree to which a crack is perpendicular to the substrate should be included in the crack's analysis.

For crack orientation, using all the points in the crack's shape is more robust than using only the two farthest points in a shape, as in Feret's diameters. A descriptor defined by all the pixels in a shape is less influenced by the presence or absence of a single pixel around the periphery [8]. The length of the crack is also an important parameter because longer cracks could produce fractures in coatings. Therefore, measurements of the maximum axis length and the angle with respect to the substrate become of great importance. Also, they can be obtained using all the points in a segment or crack using geometric moments. Further, statistical tools can be used to analyze the complete quantity of cracks in different samples of a material to compare their behavior.

Accordingly, the objective of this investigation is to present an automatic and efficient method to measure the orientation angle and major axis length of micro-cracks in images for different hard coating materials allowing the characterization of differing sample treatments.

2. MATERIALS AND METHODS

Chromium coatings were obtained from three aqueous solutions (a) Standard solution 250g/L CrO_3 and 2.5 g/L H_2SO_4 as reference, (b) 250g/L CrO_3 and 1.923 g/L H_2SO_4 and (c) 250g/L CrO_3 and 3.125 g/L H_2SO_4. The samples were steel cylinders (3cm diameter x 8cm long).

The electrodeposits were processed under different temperatures between 20 and 60°C and the current density variation was (20-60) A/dm^2. The samples were rinsed and dried after plating. They were cut to obtain smaller samples, then polished and etched with the Murakami's acid (100 g/L K_3 [Fe (CN_6)], 8 g/L NaOH, water) to develop the micro-crack pattern and to be studied by using optic microscopy. A design of experiments utilizing 2^3 for coatings was used. The cracks in the samples SA, SB, SC, and SD, as are shown in Table 1, were characterized.

Table 1. Deposit conditions.

Sample	Combination	a	b	c	a $[CrO_3:H_2SO_4]$	b (°C)	c (A/dm^2)
	-1	-	-	-	B	20	20
	a	+	-	-	C	20	20
SA	b	-	+	-	B	60	20
SB	ab	+	+	-	C	60	20
	c	-	-	+	B	20	60
	ac	+	-	+	C	20	60
SC	bc	-	+	+	b	60	60
SD	abc	+	+	+	c	60	60

For each one of the four samples, 17 microstructural images were acquired. They were captured with a Nikon epiphot 200 optical metallographic microscope which includes an integrated video system. The dimensions of the images were 640x480 pixels where 2.62 pixels represented 1μm.

The image processing consisted of two parts. The first phase was to segment the micro-cracks and the second was to measure the micro-cracks' parameters of interest. For the segmenting phase, let f be the original image and V_{gray} be the gray level that maximizes the variance between two groups of gray levels in f. The transformation g was applied to improve the uniformity of these gray levels in the cracks.

$$g(x) = \begin{cases} f(x) - V_{gray} & , \text{ if } \quad f(x) - V_{gray} \geq 0 \\ 0 & , \text{ otherwise} \end{cases}$$

An example is shown in Fig. 1. Considering Fig. 1(a) as the original image, Fig. 1(b) was the result in this step. Next, Otsu method was used to perform an intensity transformation to define a

threshold value for image g. This enabled investigators to separate cracks from the image background. Thus, the pixels are divided into two classes,

$$T(g(x)) = \begin{cases} 0 & , \ \text{if} \ \ 0 \leq g(x) \leq k \\ 1 & , \ \text{if} \ \ k+1 \leq g(x) \leq L-1 \end{cases}$$

where k is the value of intensity that maximizes the variance between classes [9,10]. The image in Fig. 1 (c) is Otsu' result of the example, after which, a filter was required. In mathematical morphology, the basic filters are the morphological opening $\gamma_{\mu B}$ and the morphological closing $\varphi_{B\mu}$ with a given structuring element (SE). B represents the elementary SE (3x3 pixels, for example) containing its origin, and μ is an homothetic parameter. Thus, the morphological opening and closing are given, respectively, by equations (1),

$$\gamma_{\mu B} = \delta_{\mu B}(\varepsilon_{\mu B}(f)) \qquad \varphi_{\mu B} = \varepsilon_{\mu B}(\delta_{\mu B}(f)) \qquad\qquad (1)$$

where the morphological erosion $\varepsilon_{\mu B}$ and dilation $\delta_{\mu B}$ are expressed as

$$\varepsilon^1_{\mu B}(f) = \inf{}_{y \in \mu B} f(x+y) \ \text{and} \ \delta^1_{\mu B}(f) = \sup{}_{y \in \mu B} f(x-y).$$

Other morphological filters are the opening and closing by reconstruction given as,

$$\tilde{\gamma}_{\mu}(f) = \lim_{n \to \infty} \delta^n_f(\varepsilon_{\mu}(f)) = \underbrace{\delta^1_f...\delta^1_f\delta^1_f}_{\text{until stability}}(\varepsilon_{\mu}(f))$$

$$\tilde{\varphi}_{\mu}(f) = \lim_{n \to \infty} \varepsilon^n_f(\delta_{\mu}(f)) = \underbrace{\varepsilon^1_f...\varepsilon^1_f\varepsilon^1_f}_{\text{until stability}}(\delta_{\mu}(f)) \qquad\qquad (2)$$

where $\delta^1_{f(g)} = f \wedge \delta_B(g)$ with $f \leq g$ is the geodesic dilation of size one and $\varepsilon^1_f(g) = f \vee \varepsilon_B(g)$ with $f \leq g$ is the geodesic erosion [9,11].

The filter applied was a morphological closing with a 3×1 line as SE. It was used to connect the disjoint cracks with vertical tendency. For the example, in Fig. 1(d) is shown as the closing result. In addition, a geodesic opening with a 3×3 square as SE was evaluated to delete the segments smaller than the SE and preserve the segments bigger than SE, as in Fig. 1(e). The size of the structuring element was chosen close to 2.62 pixels because that represents 1μm. In the closing, cracks in vertical form with that distance of separation probably correspond to the same crack. And, in the geodesic opening, particle sizes less than this were discarded because they were not considered crack, but pores. Finally, the segments that touch the edge were erased as in Fig. 1(f) to avoid biased results.

(a)

(b)

(c)

(d)

(e)

(f)
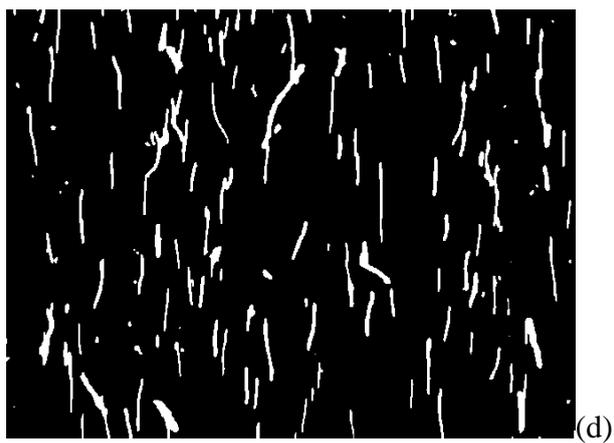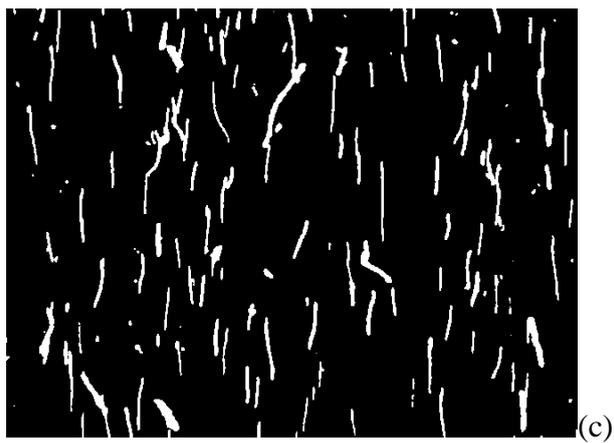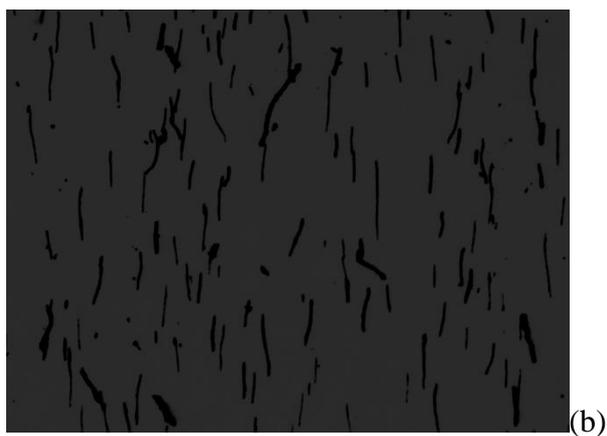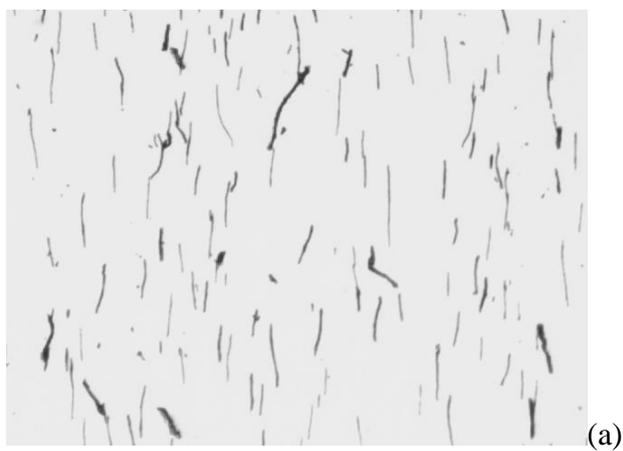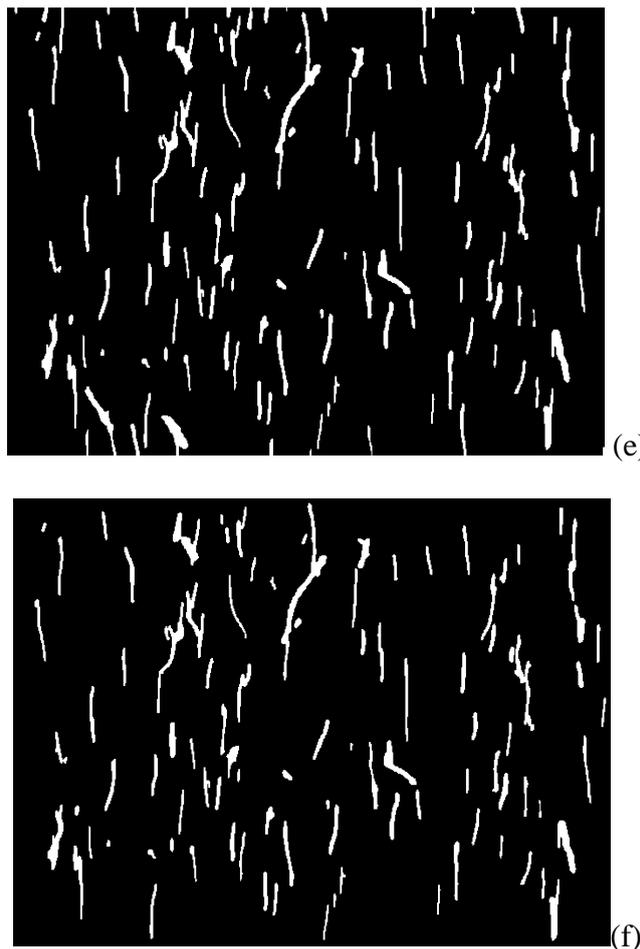
Figure 1. Operators sequence to segmentate mini-cracks in example image: (a) Original Image, (b) Subtracting max var, (c) Otsu umbralization, (d) Vertical closing, (e) Geodesic Opening, and (f) Without edge cracks.

For the measuring phase, inertia moments were used to evaluate the parameters for each crack. An inertia moment is a mathematical expression defined by the sum of the individual area elements multiplied by the square distance to its axis. It does not have physical meaning. A simple moment of order p, q is defined by equation (3), where $f(x, y)$ is the gray level in the x, y point in an image of $N \times M$ pixels.

$$m_{p,q} = \sum_{x=0}^{M-1} \sum_{y=0}^{N-1} x^p y^q f(x, y) \tag{3}$$

For a segment determined by a region S, in a binary image, the moment is defined as $m_{p,q} = \sum_{(x,y)} x^p y^q$, where (x,y) belongs to S. The object area is established as $m_{0,0}$ and the centroid $(\bar{x}, \bar{y})$ is given as $(m_{10}/m_{00}, m_{01}/m_{00})$. When the origin is moved to the centroid, the central moments of p, q order are obtained by utilizing equation (4) [12].

$$\mu_{p,q} = \sum_{x=0}^{M-1} \sum_{y=0}^{N-1} (x - \bar{x})^p (y - \bar{y})^q f(x, y) \tag{4}$$

For each crack in an image the parameters indicated below were measured:

1.   The angle θ to the ordinate axis, which represents the orientation, and
2.   the major axis length.

The angle (ϕ) of a segment defined in equation (5) is referred to as the minimum inertia axis. This is obtained through second order moments, defined either, $\mu_{20} > \mu_{02}$ if it is to the abscissa axis, or $\mu_{02} > \mu_{20}$ if it is to ordinate axis. Therefore, a transformation θ was necessary to show the perpendicularity of the segment to the substrate. If the crack angle is measured anticlockwise a positive angle is obtained and if it is measured clockwise, a negative angle is obtained.

$$\phi = \frac{1}{2} \arctan \frac{2\mu_{1,1}}{\mu_{2,0} - \mu_{0,2}} \tag{5}$$

$$\theta = \begin{cases} \phi + 90, & \text{if } \mu_{2,0} > \mu_{0,2} \text{ and } \phi < 0 \\ \phi - 90, & \text{if } \mu_{2,0} > \mu_{0,2} \text{ and } \phi > 0 \\ \phi, & \text{otherwise} \end{cases}$$

For moments, the maximum axis length $Y_{\max}$ of the segment in a binary image is defined in equation (6), with U_{xx}, U_{yy}, and U_{xy} as $\mu_{2,0}$, $\mu_{0,2}$, and $\mu_{1,1}$ normalized, i.e. $U_{xx} = \mu_{2,0}/\mu_{0,0}$, $U_{yy} = \mu_{0,2}/\mu_{0,0}$, and $U_{xy} = \mu_{1,1}/\mu_{0,0}$ respectively.

$$Y_{\max} = 2\sqrt{2} \sqrt{U_{xx} + U_{yy} + \sqrt{(U_{xx} - U_{yy})^2 + 4U_{xy}^2}} \tag{6}$$

Taking the example into consideration and Fig. 1 (f) as the last step in the segmentation, Fig. 2 (a) and Fig. 2 (b) demonstrate the length and orientation results for each segment.
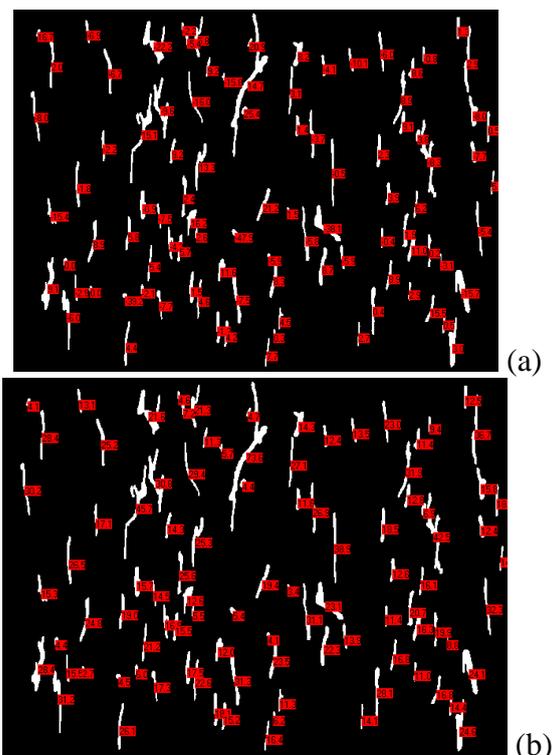
Figure 2. Measuring results in example image: (a) Angles and (b) lengths.

A manual method was performed to have measurements to compare the ones obtained with the automatic method described above. This method was implemented as follow: Four images were selected, one per sample. The cracks for each image were measured visually identifying the two extreme points per crack (x_1, y_1) and (x_2, y_2) using software that allows showing the position and the color for the location of the cursor (the software used was Jack ® Paint Shop Pro). The cartesian coordinates for the points allowed to calculate the geometric distance and angle between them. The two extreme points for each crack (x_1, y_1) and (x_2, y_2) were used to estimated the crack length l as the geometric distance between these points, $l = \sqrt{(y_2 - y_1)^2 + (x_2 - x_1)^2}$. For crack orientation, the angle θ_M in degrees was calculated as $\theta_M = -\arctan((x_2 - x_1)/(y_2 - y_1))$.

Two statistical studies were carried out to assess the effectiveness of the proposed method, one to compare the results of the proposed automatic method against the manual method and the other to evaluate the differences between the samples.
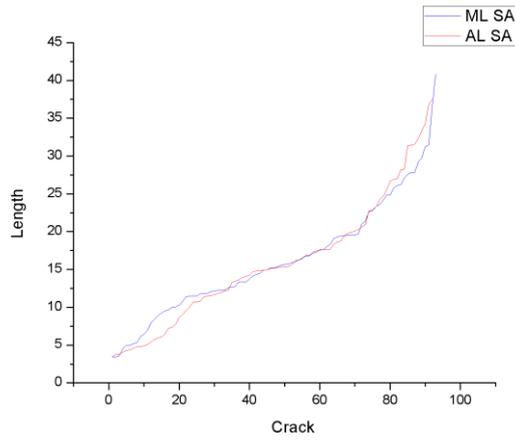
3. RESULTS AND DISCUSSION

Let us denote by AL and AA the automatic measures of the length and angle respectively, while ML and MA denote the manual ones. Two different statistical analyses were carried out. First, the proposed method was contrasted with the manual evaluation using one image for each sample. Next, the measures computed by the automatic method using 17 images per sample were compared.

Total cracks per sample were 1500 for SA, 1862 for SB, 1305 for SC, and 1660 for SD. The area per image was $44752.64\,\mu m^2$.
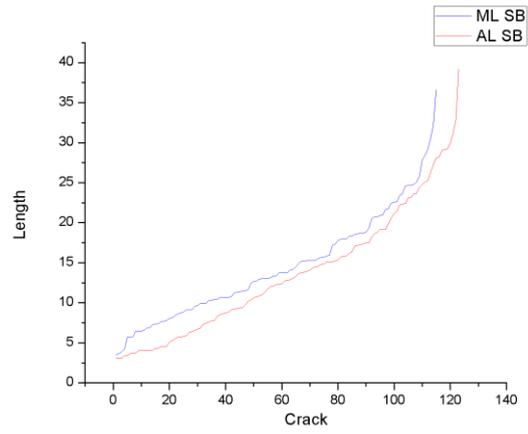
For the first comparison the images in Fig (3) were used as source and the results are presented in Fig (4) and Fig (5). These figures show the plots for the samples SA, SB, SC, and SD, where the horizontal axes are the cracks in ascending order according to the length and angle, respectively, and the vertical axes are the measurements (length and angle); the lines are red for the automatic measurements and blue for the manual measurements.
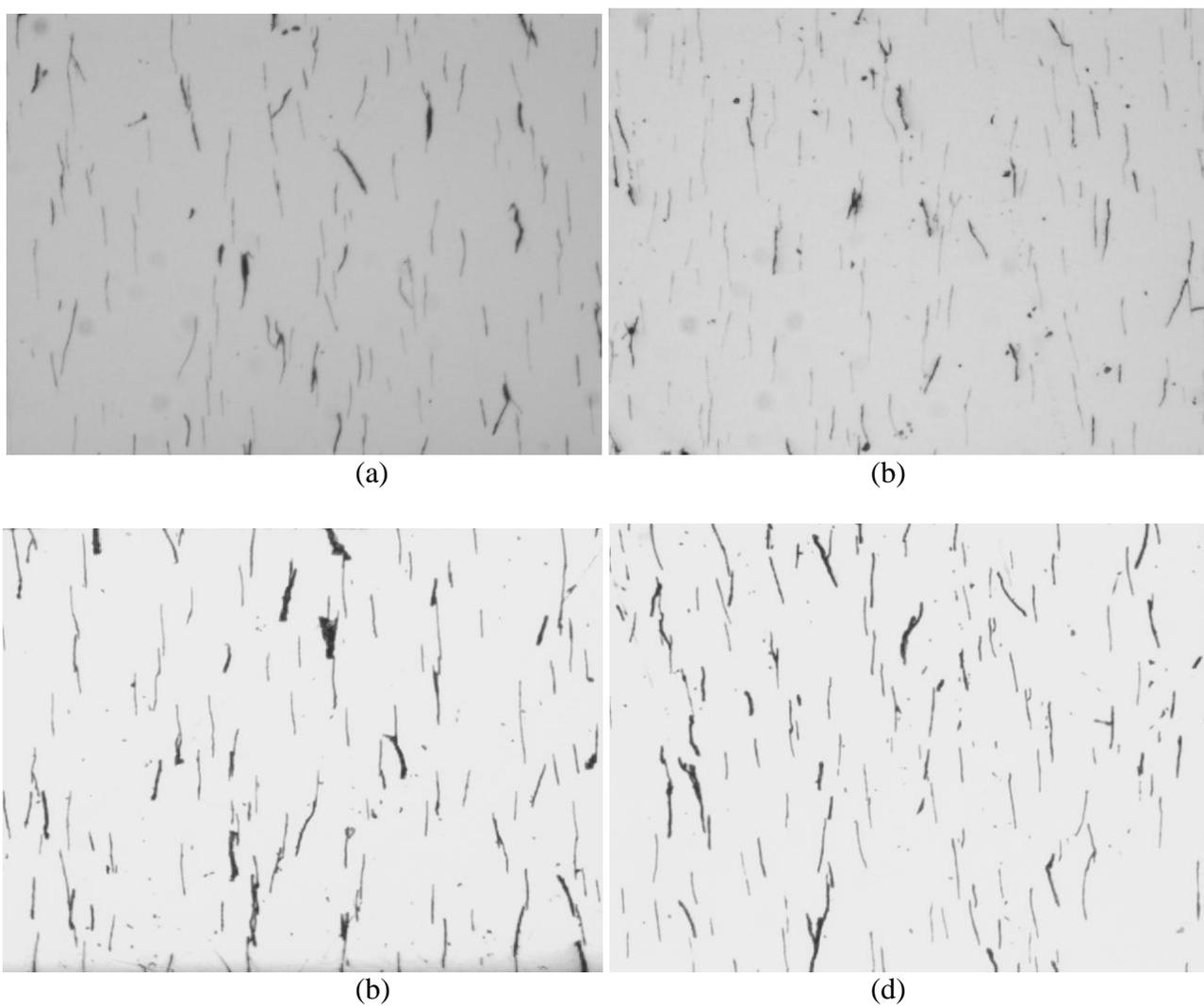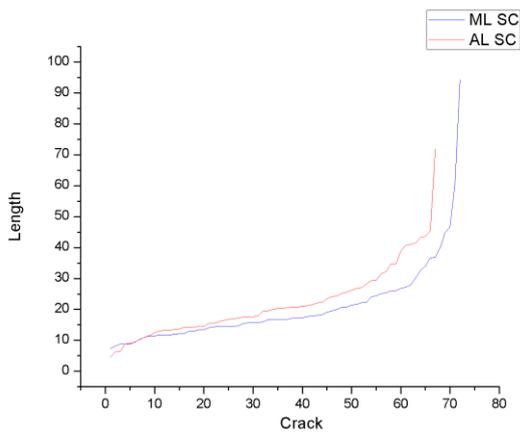

Figure 3. Images of different samples to contrast manual against proposed method measurements. (a) SA, (b) SB, (c) SC, (d) SD.
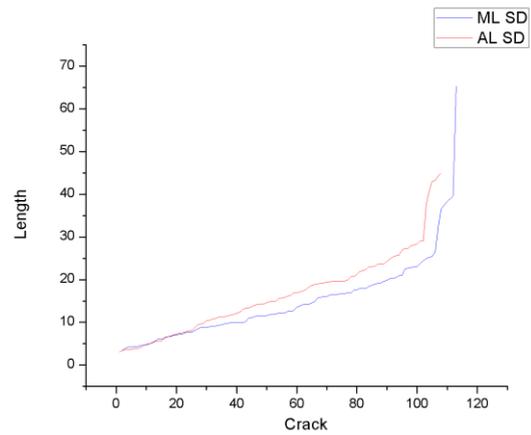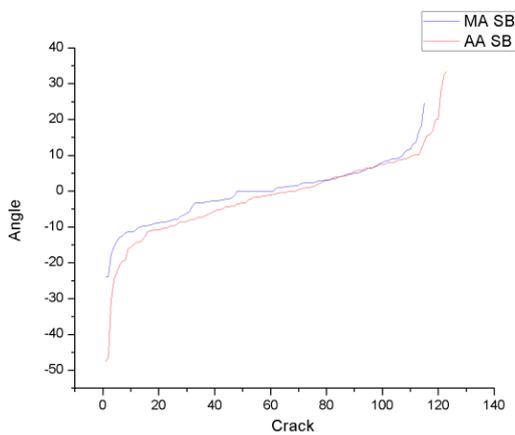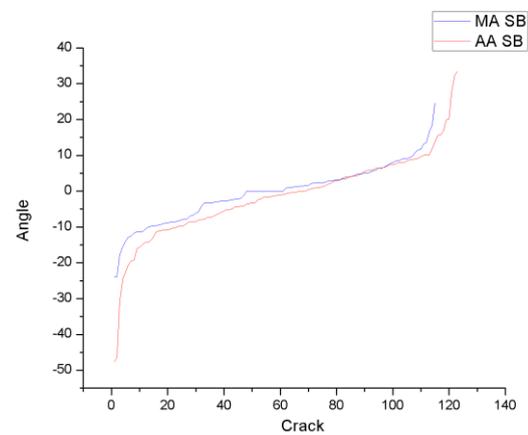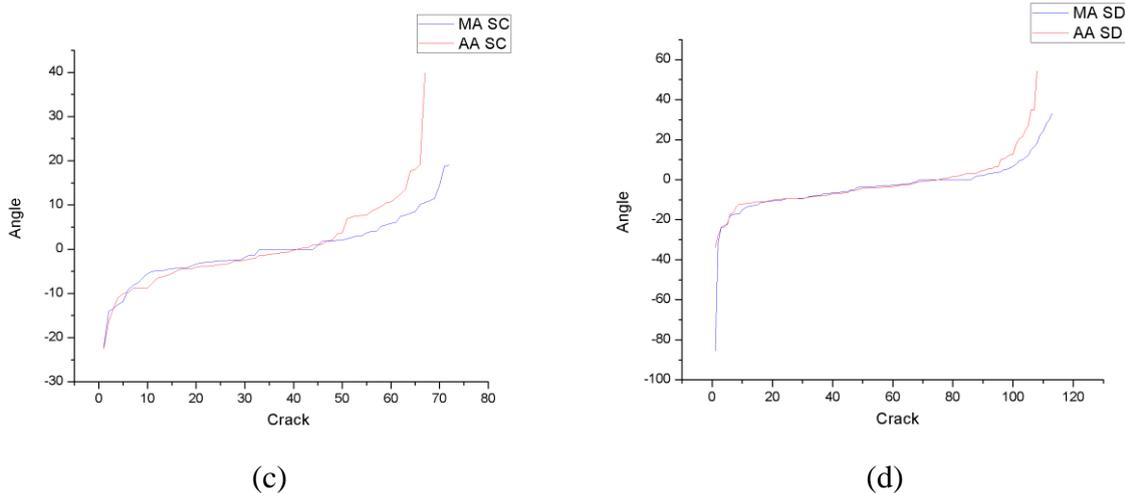
Figure 4. Length measurements for Sample A, B, C and, D. Manual against automatic method. (a) SA, (b) SB, (c) SC, (d) SD.

Figure 5. Signed angle measurements for Sample A, B, C and, D. Manual against automatic method. (a) SA, (b) SB, (c) SC, (d) SD.

The results of statistical analysis have shown that the distributions of the length and angle, for both methods (manual and automatic) were not normal. Thus, a Kruskal-Wallis non parametric test, which does not assume a normal distribution, was used for examine the data. The p-values are presented in the Table (2) considering $\alpha=.05$. These results indicate there are no significant differences between methods, because all are greater than α.

Table 2. p-values to compare manual against automatic method.

Sample	Length	Angle
SA	0.73762	0.16036
SB	0.19587	0.57124
SC	0.1971	0.56019
SD	0.09063	0.75857

Notice that with exception of sample SB, the trend was to detect more cracks in the manual method than in automatic one. It is possible that, a slight decrease in gray color within the longitudinal segment permitted the identification of two cracks while the segmenting phase in the automatic method only identified one crack as a result.
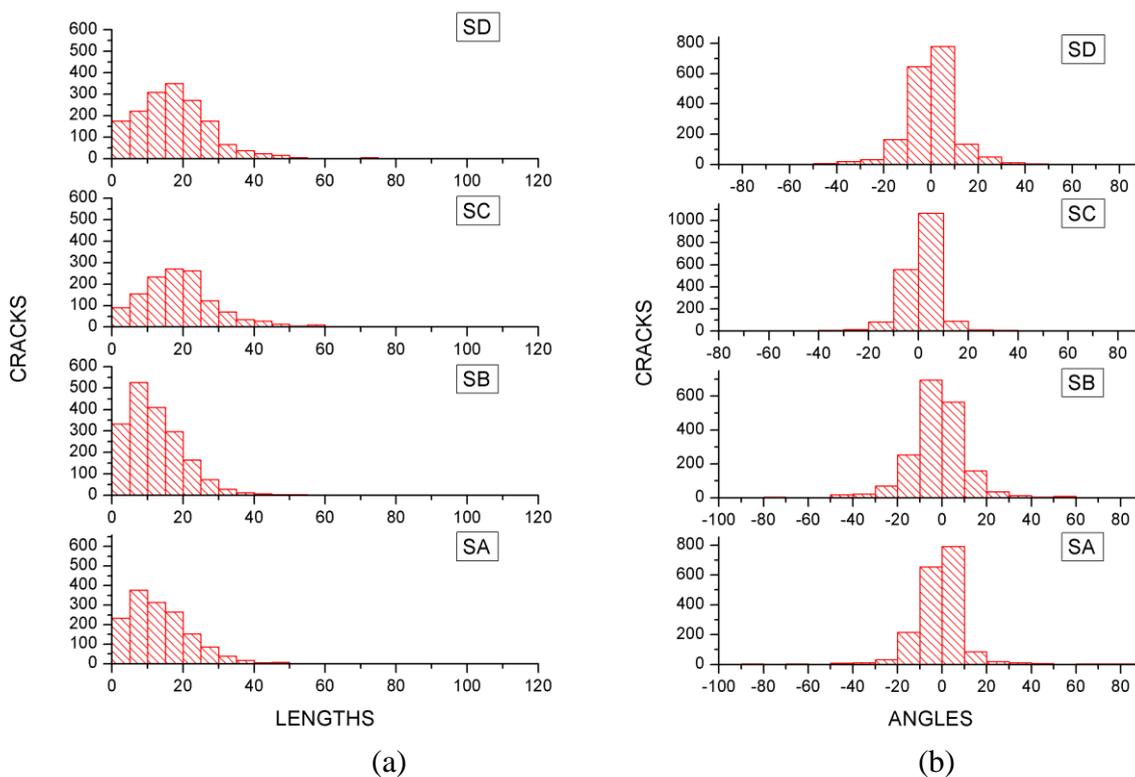
Figure 6. Measuring results for the automatic method. Four samples with seventeen images per sample. (a) Angles and (b) lengths.

Table 3. Confidence intervals for samples.

Sample	Median Length	StdDev Length	Median Angle	StdDev Angle
SA	11.694 - 13.044	9.120 - 9.797	-3.1402 - 2.1509	13.8729 - 14.9028
SB	10.274 - 11.336	7.876 - 8.399	-2.5070 - -1.3471	13.8460 - 14.7651
SC	17.432 - 18.693	10.995 - 11.872	0.7407 - 0.1368	10.6052 - 11.4517
SD	16.241 - 17.430	9.838 - 10.531	-1.0291 - -0.1153	11.8642 - 12.7000
Mood's Test p-value	< 0.001	< 0.001	< 0.001	< 0.001

On the other hand, the analyzed SB image lacked quality in comparison with the others. This image had a lot of noise, which could be incorrectly identified as cracks in the automatic method for the reviser of the images in the manual method. The differences between manual and automatic length could be due to the fact that manual measurement considers only one pair of points of the crack shape,

while the automatic method considers all points of the shape. The orientation results are more similar between manual and automatic method.

For the comparative analysis between samples the data obtained with the 17 images per sample were used with the automatic method. The results for length and angle are shown in the histograms in Fig. (6) (a) and (b) respectively. With them a general tendency of the measured parameters for the samples can be analyzed. The histograms and confidence intervals of Table (3) provide information to analyze differences between the samples.

For the statistical analysis that compares the treatments, the length and the angle were the variables used as reponses. SA, SB, SC, and SD were the four factors whose medians were compared statiscally as follow $H_0 : x_{SA} = x_{SB} = x_{SC} = x_{SD}$ for the length and the angle. The medians were compared with a Mood's Test, which is a nonparametric test, to assess such null hypothesis for the four samples in this case. The result of the test was p-value <0.001, meaning that medians for the samples are actually different, or that the null hypothesis was false; hence the samples were found statistically distinct. Therefore, there is evidence that a difference between samples exists [13]. Confidence intervals for medians were calculated at 95% confidence. The intervals showed differences in the cracks' lengths and angles per sample (see Table 3). Angles are not as well differentiated as lengths; however, the tests demonstrated clear evidence of their differences.

The Table (3) shows the confidence intervals for angles and lengths of the cracks, the samples can be differentiated based on these intervals and the sample SC has the longest cracks with the largest angles, its intervals were 17.432 – 18.693 for the median length and 0.7407 – 0.1368 for the median angle. This sample was found to present the largest effect out of the four.

The sample SB shows the shortest cracks with median in the interval of 10.274 – 11.336, however its angles were not the smallest but they were only average with median between -2.5070 – 1.3471. The sample SD shows the second longest cracks with median from 16.241 – 17.430 and the smallest angles of all the samples with median between -1.0291 – 0.1153. The sample SA shows the largest angles from -3.1402 – 2.1509 in median, but its cracks were the second smallest with median 11.694 – 13.044.

The results in Table (3) show relevant characteristics of micro-cracks in hard-coatings. By comparing the deposit conditions illustrated in Table (1), it is possible to identify the effect of the current density. That is, at low current density the effect "chicken wire" may occur [14], and in this case, the micro-cracks have small sizes and their orientations, regarding deposit orientation, also tend to disperse. Similarly, having high current densities, the size of the cracks increases and maintains a good directionality [15, 16].

4. CONCLUSIONS

The most common way to assess crack presence is the number of cracks per area. With the methodology proposed this number is automatically provided. Manual methods of measuring cracks usually report linear density or surface density regardless of the shape or orientation of the defect.

These methods are rough approximations of crack characterizations. In this investigation, an automatic method was developed and compared with a manual characterization of length and orientation of cracks; in contrast to the manual measurements that are limited to the visual accuracy and training of those who make the measurements. The proposed automatic method takes into account the whole set of points that make up the shape of the crack, so that it does not depend on external factors. This method is closer to the actual assessment of the defects in the material, which facilitates its characterization.

Comparisons are made between the methods and find that the length of the cracks using the automatic method is slightly larger. For the orientation angle the differences are smaller. The automatic method calculates the orientation based on all points in the crack while the manual method only considers two points.

The image processing methodology and the data analysis provide an accurate and automated process for cracks characterization based on two of the key variables for cracks' physical analysis. The methodology proposed, including the image processing method and the statistical analysis provides a good characterization of the cracks patterns in metal coatings. It allows better understanding of the cracks beyond the simple cracks density, adding information regarding length and angle against substrate.

References

1. M. Aroyo, D. Stoychev and N. Tzonev, *Plat. Surf. Finish.*, 85 (1998) 92.
2. N.M. Martyak, J.E. McCaskie, B. Voss and W. Plieth, *J Mat Sci*, 32 (1997) 6069.
3. R. Weil, *Plating*, 57 (1970) 1231.
4. A.R. Jones, *Corrosion of electroplated hard chromium, ASM Handbook Corrosion*, ASM International, Member/Customer Service Center, Materials Park, OH 44073-0002, USA, 13 (1987).
5. C. P. Britain and G.C. Smith, *Trans. Inst. Met. Finish.,* 33 (1956) 289.
6. H. Fry, *Trans. Inst. Met. Finish.*, 32 (1955) 107.
7. J. Grande, *Microsc. Microanal.*, 11 (2005) 1758.
8. J.C. Russ, *The Image Processing Handbook*, CRC Press, Boca Ratón, FL, USA, (2007).
9. P. Soille, *Morphological Image Analysis, Principles and Applications* 2nd ed., Springer-Verlag, Berlin, Heidelberg, New York, (2002).
10. B. Jähne, *Digital Image Processing*, Springer-Verlag, Berlin, Heidelberg, (2005).
11. L.A. Morales-Hernandez, I.R. Terol-Villalobos, A. Dominguez-Gonzalez, F. Manriquez-Guerrero and Herrera-Ruiz, G., *J. Mater. Process. Technol.*, 210 (2010) 335.
12. R. Gonzalez and R. Woods, *Digital Image Processing*, Pearson Education-Prentice Hall, Upper Saddle River, NJ, (2008).
13. W.J. Dixon and A.M. Mood, *J. Amer. Statist. Assoc.*, 41(1946) 557.

14. Grace F. Hsu, *SAE Technical Paper* 880863 (1988).
15. J. Torres-González, F. Castaneda and P. Benaben, *Theoretical and Experimental Advances in Electrodeposition*, ISBN: 978-81-308-0224-4, 101 (2008).
16. P. Benaben, F. Castañeda, R. Antaño, J. Morales, I. Terol and J. Torres-González, *Superficies y Vacío*, 25 (2012) 106.